SCA-9819

Blending Magnetic Resonance Imaging and Numerical Simulation

S. Nicula, A. Brancolini, A. Cominelli and S. Mantica

Abstract

Magnetic Resonance Imaging (MRI) has been widely used for investigation of multiphase flow in porous media. Currently, the main issue of MRI in the oil industry is the capability to obtain a quantitative evaluation of petrophysical parameters and phase saturation during core displacement experiments. While the 1D process has already been analyzed, further research should be performed on the 2D (and 3D) problems. In this paper we present the results of the post-processing conducted on MRI 2D acquisitions relative to drainage experiments at different force regimes. The raw data from MRI are processed using an interpolating model based on a continuous distribution of decaying rates. This allows the determination of petrophysical parameters and dynamical quantities. We then compare MRI saturation fronts with numerical simulations, initializing the dynamical model with the petrophysical data from MRI. In this way we validate the consistency of the experimental procedure with the data interpretation and, finally, with the numerical model.

Introduction

The investigation and simulation of the flow of two or more fluids in porous media is a key issue in the oil industry for the improvement of reservoir performance. Until the introduction of non-destructive imaging techniques (Magnetic Resonance Imaging, CT X-rays) the observation of the fluid distribution in rock and its evolution as a function of time could only be performed indirectly. Conventional methods provide only average values for such properties as porosity, saturation and permeability. NMR-based methods, in particular, have tremendous potential not only due to the capability for quantification of fluids in porous media but also due to their sensitivity to pore structure which offers a means to correlate flow properties to NMR data.

In NMR experiments, the intrinsic magnetization intensity is directly proportional to the fluid content and can be used to determine saturation and porosity distribution (Ref. 1) . By suitable modeling of the relaxation process, accurate estimates of the intrinsic magnetization intensity can be made from magnetization intensity measurement at various magnitudes of decay (Ref 2,3). Previously, multiexponential (Ref 2) and stretched exponential (Ref 4) models have been used. These methods require use of non-linear parameter estimation methods to estimate several discrete parameters. The algorithms to solve these problems are computer intensive, require a good initial guess and may fail to converge to a global minimum or at all. In imaging data analysis, where the parameter

estimation has to be carried out at a large number of pixels, such methods could prove inconvenient. A continuous distribution has been used to model relaxation at each pixel (Ref 5, 6). This provides a better representation of the relaxation process (Ref 7). Furthermore, the parameter estimation is linear so that the global minimum can be computed in a direct and robust manner. While quantitative properties, like porosity and saturation, can be directly estimated from NMR relaxation data, flow properties such as absolute permeability have to be estimated by correlation (Ref 8). These correlations relate the flow properties to NMR relaxation parameters T_1 and T_2. This study can offer an interesting development for scaling-up purposes, mainly in fields such as laminated reservoirs, where it is well-known that small scale heterogeneity is important for making decisions concerning ultimate recovery (Ref. 9).

Imaging Procedure

The NMR signal is proportional to the number of nuclei present in the analyzed region, and it is upon this effect that the method for computing porosity using NMR is based. There are several reasons that make NMR measurement and its quantitative analysis difficult. In the first group (Ref. 4) we can identify the inhomogeneities in the static magnetic field B_0, the spatial variation in the amplitude of the applied radio-frequency field B_1 and the probe loading effect as the origins of possible problems. Other difficulties arise from the effect of the relaxation processes, especially the spin-spin relaxation characterized by the time T_2. In our experiments we chose to measure a hydrogen density maps using a MRI sequence based on the CPMG (Ref. 10) method, where the decay of the NMR signal is mainly a function of T_2 time.

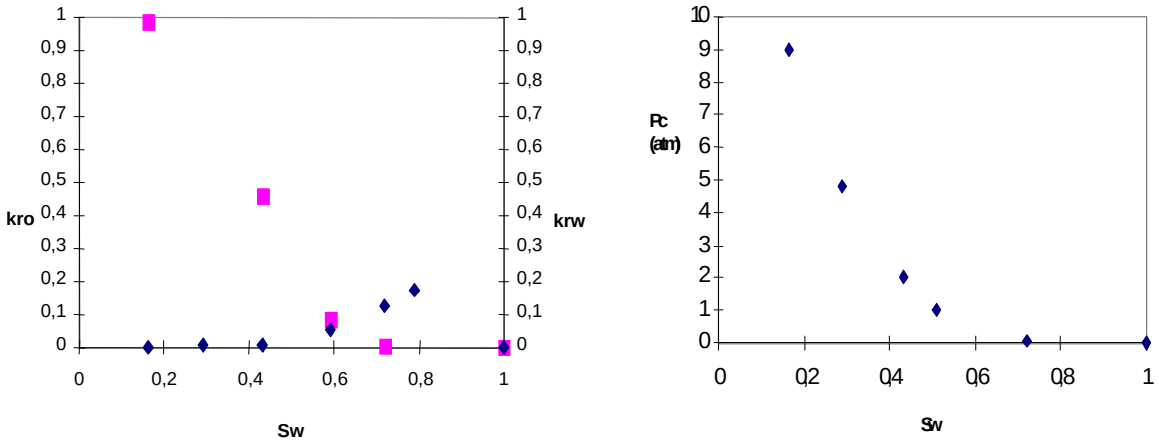

Fig. 1: Relative permeability curves (left) and capillary pressure curves (right) obtained by mean of steady state method and centrifuge method respectively.

Porosity and Permeability Estimation using MRI

A mass reference was used to convert the experimental MRI signal amplitudes into porosity. This reference has the same proton density as the fluid in the rock, so the

conversion was performed considering the porosity in the reference as 100%. Specifically, the following formula was applied:

$$\Phi_{core} = \Phi^{ref} * \frac{V_{ref} M_{core}}{V_{core} M_{ref}} \quad \textbf{(1)}$$

for each pixel in the core image, where M is the magnetization and V the pixel volume. The MRI porosity measurement can be considered as a direct measurement. However, when it comes to absolute permeability (k), NMR, for the time being at least, is reliant on calibration against independent measurements. The most practical approach is to attempt to correlate the NMR parameters for the plugs with an independently measured permeability figure. In choosing a functional relationship for the permeability of the form $k = f(F, T_{2s})$, we were guided by physical plausibility and some suggestions which have appeared in the literature. If a porous medium has all its linear dimensions scaled by a factor of q then, ceteris paribus, its porosity remains constant and its permeability changes by a factor of q^2. So, if we take T_{2s} to be the representative number for pore size, and make the simplifying assumption that our sands are changing their pore size distribution by such a simple scale then, for plugs of the same porosity, we can expect that $K \; a \; T_2^2$. No equivalent simple model exists for the dependence of k on porosity, since changing the porosity requires the pores to change their relationship to each other (in particular, the pore to pore throat size ratio will change). Combining the Kozeny model with Korringa's theory (Ref. 11) for relaxation in confined systems provides a theory for linking the relaxation times with the surface-to-volume ratio of the porous system. The following general relationship was proposed:

$$K = A\Phi^B T_2^C \quad \textbf{(2)}$$

The parameters that are shown in the formula must be calibrated. A quadratic dependence of permeability from T_2 is usually found (Ref. 12). This expression is also used in downhole log applications for absolute permeability estimations along the depth of the well (Ref. 13), and is quite effective, especially for clastic rock, where there is a link between throat dimension and pore size.

Mathematical Model – Inversion Methods

If we consider a fluid confined within a porous medium, the magnetization decay, dependent on the spin-lattice relaxation can be better described if a continuous distribution of T_2 is assumed (Ref. 7). The particular behavior of the confined fluid is due to the continuous distribution of pores inside the porous medium. The measured magnetization as a function of time can be better described as:

$$M(t_i) = e_i + \int_{t_{\min}}^{t_{\max}} P(t) e^{-t_i/t} \, dt \quad , \quad i = 1, 2, ..., n_{acqu} \quad \textbf{(3)}$$

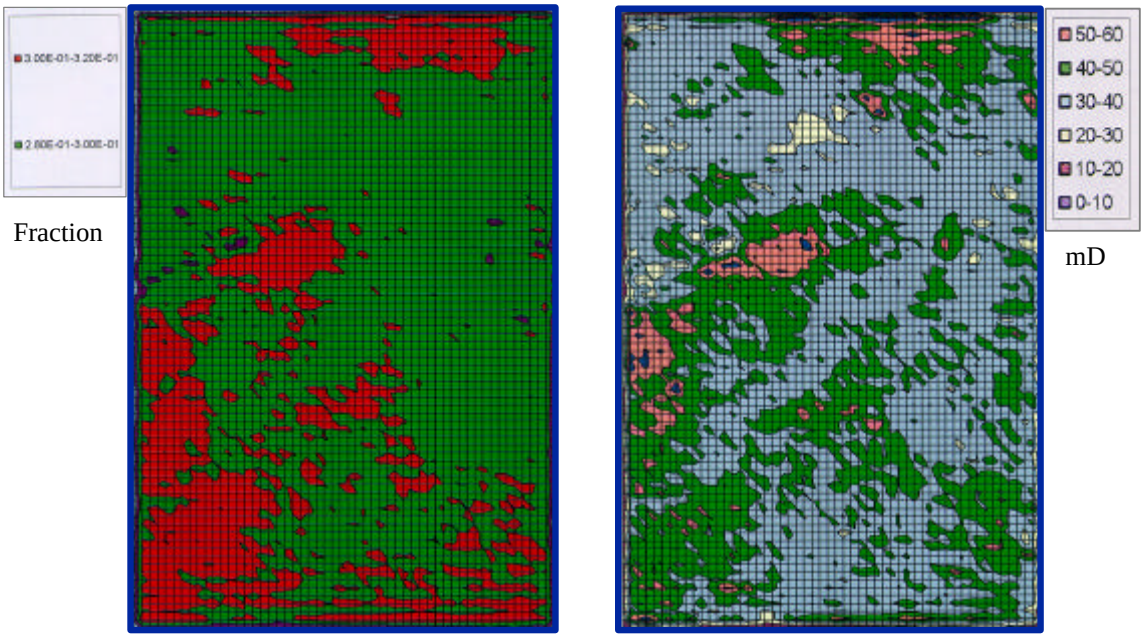

Fig. 2: Porosity Map (left) and Permeability Map (right) calculated from the NMR images.

where the distribution function $P(\tau)$ is normalized to obtain $M(0) = M_0$, n_{acqu} is the number of acquisitions and e_i is the unknown experimental noise. A finite dimension approximation of $P(\tau)$ can be written, based on the assumption of the continuity of the distribution of pores.

MRI acquisitions

Static and dynamic MRI experiments were conducted using a Bruker BIOSPEC 24/40 instrument equipped with a 40 centimeter bore superconducting magnet with a gradient strength of up to 50 mT/m. A variety of MRI acquisition sequences can be used to obtain spin density images of variably saturated core plugs. Sequences based on images acquired with a single echo at increasing echo times (TE), in order to construct decay curves, have the drawback of sensitivity to diffusion effects, and are usually quite difficult to manage. In this study a multi-slice multi-echo (MSME) sequence, based on CPMG method, has been used. A key factor in this kind of experiment is the constant TE, which must be kept as short as possible. An optimal value for TE is the result of a compromise between the size of the acquisition matrix and the resolution of the image. In our acquisitions the value of TE was 4.8 ms. The static measurements consisted of the determination of the porosity map of the sagittal slice of the sample and the calculation, by correlation, of the absolute permeability map of the same slice. The dynamic study that allows one to visualize the advancement of the front and determinate the saturation of the two phases as a function of time. Every NMR image lasted 2 min. and the front may be approximated as being stationary during this short time delay. The additional petrophysical parameters were available, such as capillary pressures, and measured for the case of a “wetting” phase

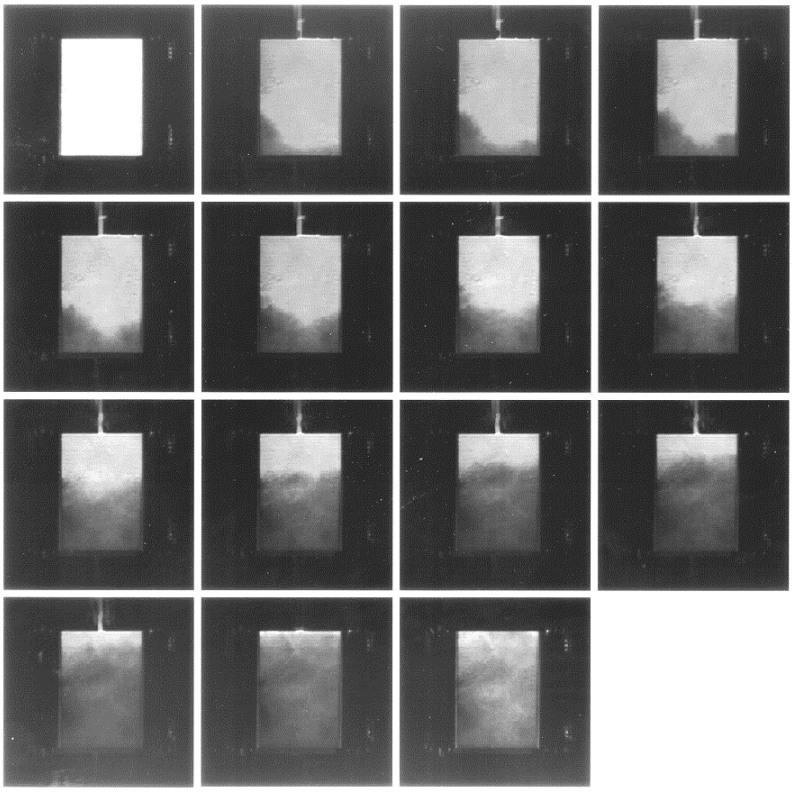

Fig. 3: The displacement experiment visualized by NMR imaging. An image was recorded every 20 min. The "breakthrough" time was detected to be after 175 min.

displaced by a "non-wetting" one. The image resolution was 700 μm/pixel and at the same resolution were calculated the maps of the petrophysical parameters and the saturation during the displacement. The thickness of the virtual sagittal slice was 5 mm. The measurements were done using a plug of 3.9 cm diameter and 5.3 cm length.

Its porosity obtained by conventional core analysis methods was 29% and its permeability with respect to air was 37 mD. The sample was selected as being homogeneous by doing an initial qualitative NMR image. The average porosity calculated from a sagittal NMR slice was 28.6%. In reality, as visible in the porosity and permeability maps (Fig.) a certain heterogeneity exists even if not elevated. The water that saturates initially the sample had the same salinity as the formation brine, of 60 g/l. In order to be able to distinguish between the two liquid phases flooding the plug, a fluorated oil was used. Its viscosity was 20 cp. The substitution of the hydrogens with the fluorine atoms avoids the oil giving a NMR signal at the proton Larmoor frequency. This way the only visible liquid inside the plug, from the NMR part of view, was the water. The experiments were performed at ambient conditions and consisted of the displacement of the water that initially saturated the sample with the oil. The flow rate was constantly fixed at 0.05 cc/min (0.3m/g). The breakthrough moment of the oil was detected to be after 175 min.

The decay curves, at each pixel in the image, were fitted with both the least square exponential (LSE) model and the TAMU model to obtain M_0 and T_2^{avg}. The porosity and permeability maps were subsequently computed using Eqs. (1) and (2). Permeability MRI maps were compared to minipermeameter (NER, Vermont, USA) data in order to validate the reliability of the procedure. Low field NMR measurements were done with a MARAN-2 (Resonance Instrument, Oxford, UK).

Simulations

In order to simulate the displacement, we applied the mathematical model ECLIPSE 100 (version 96A). As already pointed out, the application of a reservoir simulator to the plug size needs some additional inputs particularly for the definition of the faces of input and output of the fluid. The relative permeability curves, k_r, and capillary pressure, P_c, are presented on Fig. 1 and were calculated by means of classical methods: centrifuge method for P_c and both steady state and unsteady state methods for k_r. For the simulation the steady state assumption was used. The porosity and permeability maps were obtained from the Nuclear Magnetic Resonance-NMR images, the last one being calculated doing a correlation similar to the one used for the calculation of the absolute permeability and expressed on Eq. 2. The number of cells used for the simulation matches the number of the pixels of the NMR image and was 79 on the *x* dimension and 54 on the *y* dimension. The two dimensional assumption of the displacement was important for the numerical simulation taking into account that all the process defining the shape of the front was confined within the volume imposed by the virtual slice recorded by MRI.

Results and Discussion

The MRI technique is already certified as being capable to quantify the variation in fluid saturation as function of time during a displacement experiment performed inside the Magnetic Resonance Imager. In the case we are presenting here the advancement of the oil phase was monitored in the sagittal slice of the plug initially saturated with water. The saturation maps quantify the amount of water present in each cell and its variation with respect to the initial situation. The volume of the cell was imposed by the MRI resolution to be 0.7x0.7x5.0 mm. A quantitative control was possible in order to evaluate the error induced by the calculation of saturation from MRI relative to the values obtained by weighting methods and reported on Tab. 1. Unfortunately for the intermediary steps characterized by a mixed phase at the exit face it was impossible to achieve the individual detection of each phase. A phase type discrimination is possible under certain conditions doing Chemical Shift Imaging – CSI. In our case the chemical shifts of the water and oil being very close one to another makes the quantification of the two phases impossible. The displacement experiment was monitored by recording an image of the same sagittal slice every 20 min. In Fig. 3 is depicted the advancement of the oil front. It can be seen that the front splits and advances more rapidly in the region for which the porosity and permeability maps illustrated on Fig. 2 presents highest values (bottom left-hand side). At the half time

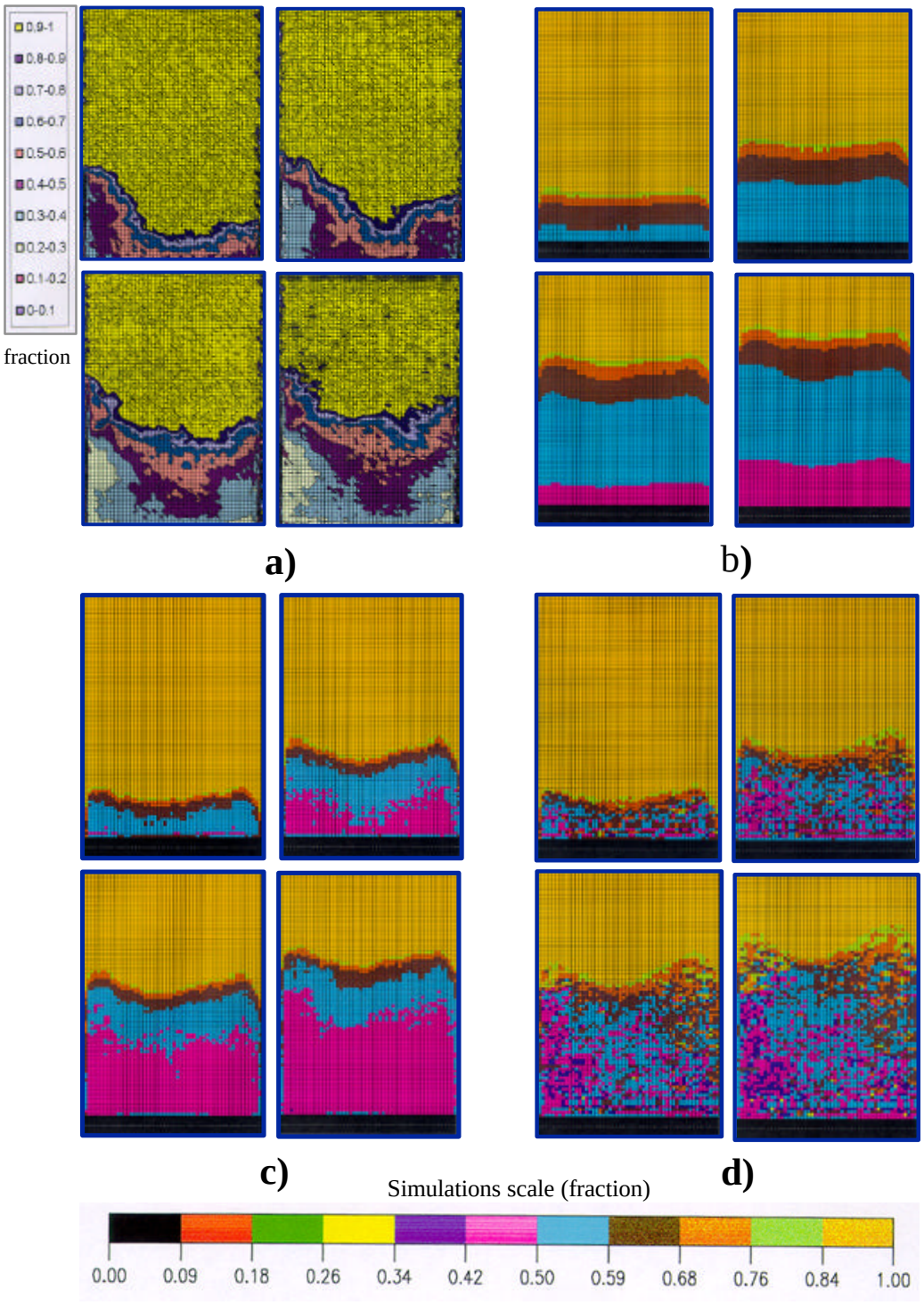

Fig. 4: Water saturation maps at times 30, 60. 100, and 120 min. of displacement: **a)** calculated from NMR images; **b)** simulation using for all the cells an identical set of P_c and $k_{r.}$; **c)** simulation using a scaled set of P_c.; **d)** simulation of the same displacement experiment as in Fig. 5 using a scaled set of P_c and S_{wi}.

of the experiment this "fingering" effect related to the inhomogeneity of the rock is attenuated and the displacement reaches a "piston" regime, affected by a mobility factor smaller than unity.

Experimental Time (min.)	Average Water Saturation By MRI (%)	Average Water Saturation by Weighting (%)	Error (%)
30	94	91	3
60	88	83	6
100	78	72	8
120	73	66	11
300 (final S_w)	37	35	6

Tab. 1: Water saturation calculated at different times and the error estimation of the values obtained from MRI with respect to the classical weighting method.

Responsible for this effect is the homogeneity in porosity and permeability of the region spatially situated in the middle of the sample as visible on Fig. 2. We can conclude that small differences in permeability and porosity have an important impact on the advancement front. Fig. 4a represents the 2D maps of the water saturation calculated from MRI for the four steps mentioned on Tab. 1. In order to match the numerical simulations with the experimental results obtained from MRI several inputs were used on three different simulations. Fig. 4b shows the results of the simulation where for all the cells were used an identical set of flow functions (P_c and k_r). We should note that the front has a flat shape slightly curved on the areas of equal saturation. The "breakthrough" time is anticipated to be 160 min. It seems that with these inputs the simulator cannot simulate the reality in an accurate way. In order to improve the results we repeated the simulation allocating this time a local value of capillary pressure for every cell. The P_c values were scaled to the local values of permeability and porosity treating the initial capillary pressure curve using the "J – function" approach (Ref. 16). The result is reported on Fig. 4c showing that the oil front simulated reproduce accurately the experiment even if it doesn't have the same behavior on its left-hand side. The "breakthrough" time matched the experimental one being calculated at 175 min. The final situation after 5 hours of displacement is shown in Fig. 5. On the left-hand side is depicted the water saturation calculated from NMR images while on the right-hand side is visible the simulation of the same situation. The two saturation maps have a similar shape, a fact that validates the simulation inputs. It should be noted that for the simulation was used a single value of S_{wi} equal to 16% calculated by way of classical methods. The average water saturation S_w simulated was 33% while the measured value was 35%. The last step of our simulations consisted of a scaling of Swi together with the P_c in order to describe the local variation in S_{wi}. The final water saturation map obtained by MRI after 5 hours of displacement were used as a reference. The shape of the front was similar to the one obtained previously by scaling only the local P_c; however the "breakthrough" time was simulated to be at 150 min. This may confirm the fact that, after 5 hours of displacement, the sample was not at S_{wi} condition. The result of this simulation is shown of Fig. 4d.

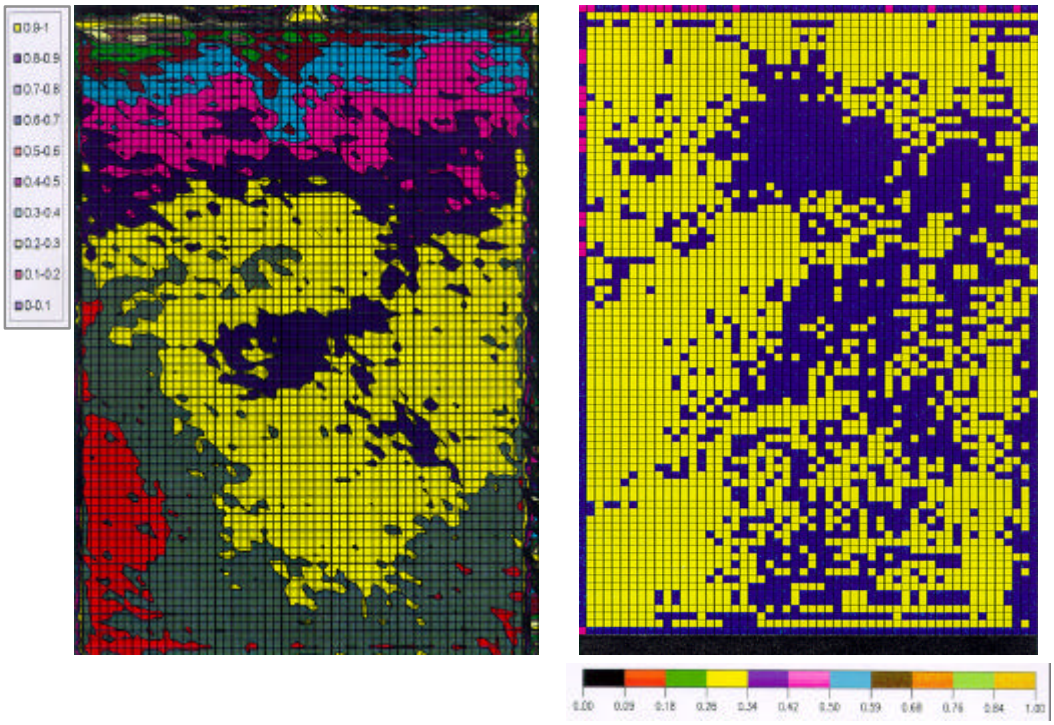

Fig. 5: The final water saturation maps calculated from NMR image (left) and simulated with ECLIPSE (right).

Also the simulation of the average water saturation give values higher than the experimental reality (38%). In conclusion the important contribution to the improvement of the simulation of displacement experiments was the allocation of local values for the capillary pressure P_c.

Conclusions

Magnetic Resonance Imaging allows the computation of two-dimensional maps of petrophysical properties. Millimetric scale porosity can be determined once precise values for intrinsic magnetization intensity have been computed. The integration of the great potential of the NMR imaging into simulations may improve the understanding of the influence of the petrophysical parameters on fluid dynamics inside the porous media.

Permeability is estimated from the correlation that exist between the relaxation times and the pore size distribution. This requires a calibration process, such as that performed for downhole logs. We have observed that the T_2 effect, in terms of the improvement of the permeability estimation in relation to the usual *K-F* cross plots, is not as evident as at low field. The availability of this huge quantity of data on the core scale allows us to produce histograms and semi-variograms of the parameters being investigated. This way the statistical approach, which is usually applied in the field, can be transferred to a lab scale to investigate any similarities.

Aknowledgements

We are indebted Eni SpA for giving the permission to publish this work. Special thanks are due to A. T. Watson for the many helpful discussions we had on the subject presented here.

References

1. Mandava, S. S., Watson, A. T., Edwards, C.M.: “NMR Imaging of Saturation During Immiscible Displacements,” AIChE. J., 36, 1680 (1990).
2. Chen, S. F., Qin, K. H., Watson, A. T.: “NMR Imaging of Flow in Porous Media,” AIChE. J., 39,925 (1993).
3. Chen, S. F., Qin, K. H., Watson, A. T.: “Determination of Fluid Saturation During Multiphase Flow Experiments Using NMR Imaging Techniques,” AIChE. J., 40, 1238 (1994).
4. Lucas, A. J., Pierens, G. K., Peyron M., Carpenter, T. A., Hall, L. D., Stewart, R. C., Phelps, D. W., Potter, G. F.: “Quantitative Porosity Mapping of Reservoir Rock Cores by Physically Slice Selected NMR”. In: P. F. Worthington, C. Chardaire-Rivière (Eds.). Advances in Core Evaluation III: Reservoir Managment. Gordon and Brench; 1993.
5. Liaw, H. K., Kulkarni, R. N., Chen, S., Watson, A. T.: “Characterization of Fluid Distributions in Porous Media by NMR Techniques”, AIChE J., 42, 538 (1995)
6. Kulkarni, R. N., Watson, A. T., “A Roboust Linear Techniques for Quantification of NMR Imaging Data,” AIChE J., in press 1997
7. Brownstein, K. R., Tarr, C. E.: “Spin-Lattice Relaxation in a Spin Governed by Diffusion”, J. Mag. Reson., 26, 17 (1977)
8. Seevers, D. O. “A Nuclear Magnetic Method for Determining the Permeability of Sandstones”, Trans. SPWLA 6, Sec. L; 1966.
9. Ringrose, P. S., Sorbie, K. S., Corbett, P. W. M., Jensen, J. L.: “Immiscible Flow Behaviour in Laminated and Cross-Bedded Sandstones”, JPSE, 9 (1993) 103-124.
10. Callaghan T. P. (1991), “Principle of Nuclear Magnetic Resonance Microscopy”, Oxford Science Publications.
11. Kenyon, W. E., Day, P. I., Straley, C.:“A Three-part Study of NMR Longitudinal Realxation Properties of Water Saturated sandstones”, SPEFE, 3, 622-636; 1988.
12. Borgia, G. C., Bortolotti, V., Brancolini, A., Brown, R. J. S., Fantazzini, P.: “Developments in Core Analysis by NMR Measurements”, Magn. Res. Imag., Vol 14, No 7, 1996.
13. Brancolini, A., Gossenberg, P., Lyne, A., Mackenzie, I. S., Radaelli, F.: “The Use of NMR Core Analysis in the Interpretation of Downhole NMR Logs”, SPE 30559 presented at the An. Tec. Conf. & Ex., Dallas 22-25 Oct., 1995
14. Hohn M. E. (1988), “Geostatistics and Petroleum Geology”, Van Nostrand Reihold
15. Malick, K. M., Hewett: “Boundary effects in the Successive Renormalization of Absolute Permeability”, 7th SCRF Annual Report, Standford, 1994.
16. Leverett, M. C., “Capillary Behavior in Porous Solids”, AIME (1941), 152-169.